Available online at www.sciencedirect.com
ScienceDirect
Journal of Sound and Vibration 302 (2007) 287–312
JOURNAL OF SOUND AND VIBRATION
www.elsevier.com/locate/jsvi

Effect of fan outlet guide vane on the acoustic treatment design in aeroengine nacelle

X. Sun*, Z. Yang, X. Wang

School of Jet Propulsion, Beijing University of Aeronautics & Astronautics, Beijing, PR China

Received 13 April 2006; received in revised form 29 November 2006; accepted 3 December 2006
Available online 16 January 2007

Abstract

The main objective of this study is to clarify the effect of the outlet guide vane (OGV) on the acoustic treatment design in aeroengine nacelle, which received less attention previously. A model of sound propagation through a lining section and a blade row is developed to investigate the interaction between sound sources of blade rows and liners in a channel of parallel walls containing uniform mean flow. The present method makes it possible to evaluate the performance of liner while a blade row is inserted in the channel and the sound attenuation in a duct with both liner section and cascade. Various numerical results show that the effect of the cascade may have diverse effects on sound attenuation of the liner under different conditions, but the existence of the OGV always enhances the total sound attenuation in the duct due to energy dissipation caused by vortex shedding from the tailing edge of the OGV. To pursue a better design of acoustic liner in aeroengine nacelle, it is thus necessary to include the effect of OGV on the sound attenuation.
© 2006 Elsevier Ltd. All rights reserved.

1. Introduction

With the development of high bypass ratio turbofan engines, the contribution of fan has played a very important role in the overall noise of aircraft [1]. A lot of effort has been paid to noise suppressor design, especially the design of acoustic treatment in aeroengine nacelle, as seen in Fig. 1. Generally, the acoustic liner on nacelle can be partitioned into three sections. For the liner Section 2, the sound waves generated by rotating fans propagate downstream through this liner section; on the other hand, the sound waves generated by the OGV due to wake would propagate upstream through this section too. In the general methods to design acoustic liners, such as the finite element method, numerical simulation methods based upon computational aeroacoustics (CAA) technique and the mode-matching method, the sound source is always treated as a strength-fixed source. However, for the case in Fig. 1, if one does not consider the effect of OGV on the sound attenuation in the duct, the accuracy of the design of liners for noise reduction would be suspectable. To author's knowledge, there is few work available in current literature to investigate this problem. The difficulty lies in how to describe the interaction between the sound sources and acoustic liners. This is in fact a quite complicated problem. Therefore, in order to get more insight into the mechanism related to the interactions,

*Corresponding author. Tel.: +86 10 82317408; fax: +86 10 82317408.
E-mail address: sunxf@buaa.edu.cn (X. Sun).

0022-460X/$ - see front matter © 2006 Elsevier Ltd. All rights reserved.
doi:10.1016/j.jsv.2006.12.004

Nomenclature

b	blade semichord
c_0	sound speed
G	Green's function in the duct
h	height from the hub side to the tip side in the transformed space
h_1	stagger distance, measured parallel to chord
h_2	gap distance, measured normal to chord
k_0	wavenumber
k_n	wavenumber in ζ-direction
$k_{m,n}$	radial wavenumber of mode (m,n)
m	spinning mode order
n	radial mode order
p	acoustic pressure
$\bar{p}$	amplitude of perturbation pressure
$\bar{v}$	upwash velocity of the reference blade
p_d	disturbance acoustic pressure
p_i	acoustic pressure of incident sound wave
$\vec{r}$	vector coordinate
$\vec{r}_0$	vector coordinate denotes the mass source singularities
t	time in an observer point
v_b	normal vibration velocity of blade
x, y, z	an orthogonal coordinate system for an observer
x_0, y_0, z_0	an orthogonal coordinate system for an source
x', y', z'	a duct-fixed coordinate system
H	height from the hub to the tip side
K	kernel function
l	axial length of liner reduced by blade chord
M_r	Mach number in chordwise direction
U_r	mean velocity in chordwise direction
U	mean velocity in x'-direction
V	mean velocity in y'-direction

Greek letters

α	wavenumber in ξ-direction
β	wavenumber in η-direction
θ	blade stagger angle
Λ_0	eigenfunction normalizing factor
$\delta(\cdot)$	Dirac Delta function
$\gamma^{\pm}_{m,n}$	axial wavenumber of mode (m,n) for liner section
$\Phi_{m,n}(y,z)$	eigenfunction of a hard duct
$\Phi^*_{m,n}(y,z)$	conjugate form of $\Phi_{m,n}(y,z)$
σ	interblade phase angle
ρ_0	mean density
ρ'	acoustic density
τ	time associated with emission of sound wave; time delay
μ	radial mode number for incident sound wave
ω	angular frequency reduced by c_0/H
ω_0	dimensionless characteristic angular frequency of the facing sheet
ω_b	perturbation frequency of blade force
$\Delta\bar{p}$	amplitude of pressure difference

we will discuss a simplified model shown in Fig. 2. It is obvious that the key to study the interaction is to set up a model, which includes the effect of a blade row on the acoustic treatment design.

It is noted that there are many investigations that focus on either the sound attenuation through a duct with acoustically lined wall or the sound propagation through a blade row. In fact, the problem of wave propagation in ducts with acoustically lined wall has been studied in a lot of previous work. Effects of wall admittance changes on duct transmission and radiation of sound has been investigated by Lansing and Zorumski [2] and Unruh [3] by use of mode-matching matrix technique; and Koch [4] explored sound attenuation in multielement acoustically lined rectangular ducts by use of Wiener–Hopf technique. Namba and Fukushige [5] presented the method of singularity for analysis of the acoustic field in a partially lined duct, which is applicable to non-uniform lined wall in the stream-wise and/or circumferential direction. Besides these methods, the finite element method has been suggested to calculate the sound propagation in lined flow ducts by Eversman [6], and the numerical simulation method based on CAA technique [7,8] has been developed for the prediction of the sound propagation and radiation from a lined duct.

On the other hand, the propagation of sound waves through a blade row has been investigated by Kaji and Okazaki [9] based on the semi-actuator disk theory, meanwhile Kaji and Okazaki [10] suggested a more sophisticated and exact acceleration potential method. A good agreement with each other for small blade spacing is given in their works. Then the semi-actuator disk model was applied to sound transmission calculations including three-dimensional incident sound field and multiple blade rows in turbomachinery by

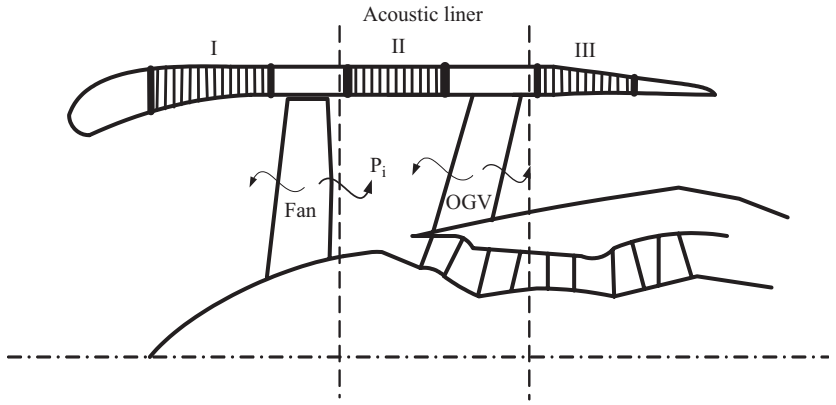

Fig. 1. A schematic of aeroengine Nacelle.

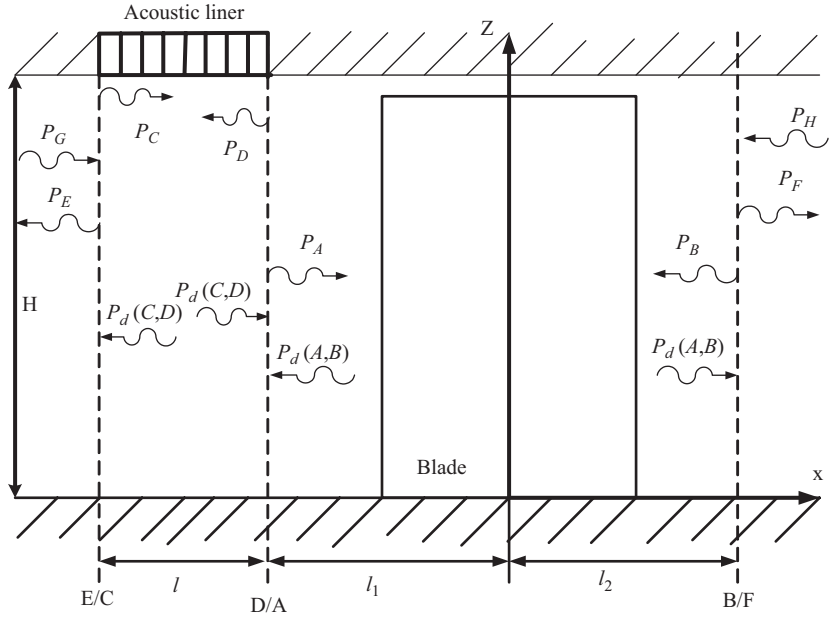

Fig. 2. Analysis model for OGV and lined wall Section 2.

Muir [11,12]. Using the Wiener–Hopf technique, Koch [13] obtained more accurate results of the reflection and transmission problems. Amiet and Sears [14] used the method of matched asymptotic expansions, in which the blade force was calculated by using quasi-steady Prandtl–Glauert theory. Whitehead [15] developed a calculation method applicable to the transmission and reflection problems, and to the generation of sound waves by vibration and incoming flow disturbances, based upon the work of Lane and Friedman [16]. All the methods are in good agreement with the results of Kaji and Okasaki [10].

However, it is noted that the current design models for a duct acoustic liner are based on a strength-fixed sound source without including the effect of the liner reaction to the sound source. For practical application, liners and blade rows often work in the same duct simultaneously. It is essential to consider effect of the interaction between liner and blade sound source in the preliminary design for aeroengine noise control. Therefore, the main purpose of this study is to clarify how a blade sound source interacts with a liner section, and investigate the possibility to design an optimum combination of acoustic liners and the OGV.

In the present work, an acoustic model of cascade airfoils in a three-dimensional subsonic flow field is presented, in which the blade row and liner section are treated as independent elements, respectively. For the liner section, the spinning mode eigenfunction expansions is still used here to obtain the solution of sound field in the duct, while the effect of lining wall is modeled by series of monopole sources suggested by Namba and Fukushige [5], which effectively avoids solving a complicated complex eigenvalue problem. For the blade row section, each blade is treated as an unsteady distribution of pressure doublets, which is suggested to calculate the amplitude of sound waves by Kaji and Okazaki. Given a known input upwash perturbation [17,18], an upwash integral equation for the unknown doublet distribution function can be derived by use of the condition that there must be no net upwash at the surface. Considering the eigenfunction still meet the orthogonal condition in the present case, a solution is constructed for a given lined duct element or blade row element with arbitrary axial length and position, which has the interface parameters as unknown variables. With this special mathematical treatment, a solution for an infinite-length duct has been extended to that for a finite-length duct element no mater what sound source is, dipoles like a blade row or monopoles like an acoustic liner. It is found that it is particularly useful to construct such an element solution to make full use of the existing mode-match technique [19]. The present model is thus powerful in describing the effect of reflective sound waves on blades under the soft wall condition and is capable of giving the physical interpretation to the interaction between lined wall and blades. Various numerical results are presented to show the effects of wall impedance on sound propagation through a blade row, and the effects of the blade row on sound propagation through the finite-length lined wall section.

2. Formulation of the problem

2.1. Analytical model and basic solutions

The following analysis is based upon the assumption of a compressible, inviscid, thermally non-conducting fluid, three-dimensional system with subsonic uniform flow parallel to the blades, which are flat plates of negligible thickness, and with small perturbations superimposed. In addition, the Kutta–Joukowski condition for unsteady flow is satisfied at the trailing edge, and the lower plate (hub side) and upper plate (tip side) as shown in Fig. 2 are assumed rigid. The uniformly moving medium wave equation is

$$\nabla^2 p - \frac{1}{c_0^2}\frac{D_0^2 p}{D\tau^2} = -\gamma(\vec{r}', \tau), \tag{1}$$

where $\gamma(\vec{r}', \tau)$ represents the source distribution. According to the generalized Green's function theory [20] the equation can be written as

$$\nabla^2 G - \frac{1}{c_0^2}\frac{D_0^2}{D\tau^2} G = -\delta(t-\tau)\delta(\vec{r} - \vec{r}'). \tag{2}$$

The corresponding boundary condition is assumed to satisfy

$$\frac{\partial G}{\partial n} = 0 \ \text{ if } \vec{r}' \text{ on the tip or hub side of the duct.} \tag{3}$$

If we consider a moving source with a volume of $\upsilon(\tau)$, surface area of $s(\tau)$ and a velocity of V, Goldstein [20] has shown

$$\begin{aligned}\rho'(\vec{x}, t) = {} & \frac{1}{c_0^2}\int_{-T}^{T}\int_{\upsilon(\tau)} \frac{\partial^2 G}{\partial y_i \partial y_j} T'_{ij}\, \mathrm{d}\vec{y}\, \mathrm{d}\tau \\ & + \frac{1}{c_0^2}\int_{-T}^{T}\int_{s(\tau)} \frac{\partial G}{\partial y_i} f_i\, \mathrm{d}s(\vec{y})\, \mathrm{d}\tau + \frac{1}{c_0^2}\int_{-T}^{T}\int_{s(\tau)} \rho_0 V'_n \frac{D_0 G}{D\tau}\, \mathrm{d}s(\vec{y})\, \mathrm{d}\tau,\end{aligned} \tag{4}$$

where T'_{ij} denotes a volume quadrupole source, f_i denotes a dipole source, $\rho_0 V'_n$ denotes a monopole noise source.

In the model as Fig. 2 shows, the liner is considered as a series of monopole sources, and the blade row is treated as a series of dipole sources or doublets. The effect of quadrupoles is assumed to be neglected in the present model (Fig. 3).

2.2. Formulation for the blade row section

As shown in Fig. 4, a cross-section is also assumed both on the left side and on the right side of the blade row, and then we get a separate element for analysis. To the blade row section, Goldstein [20]

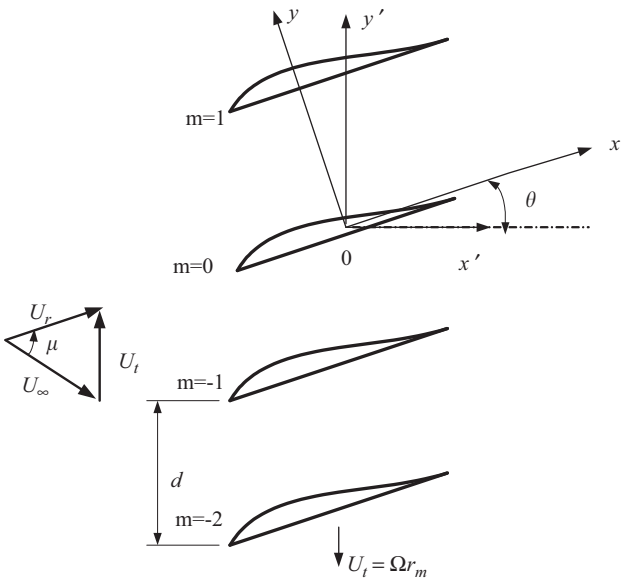

Fig. 3. Coordinate for one blade row.

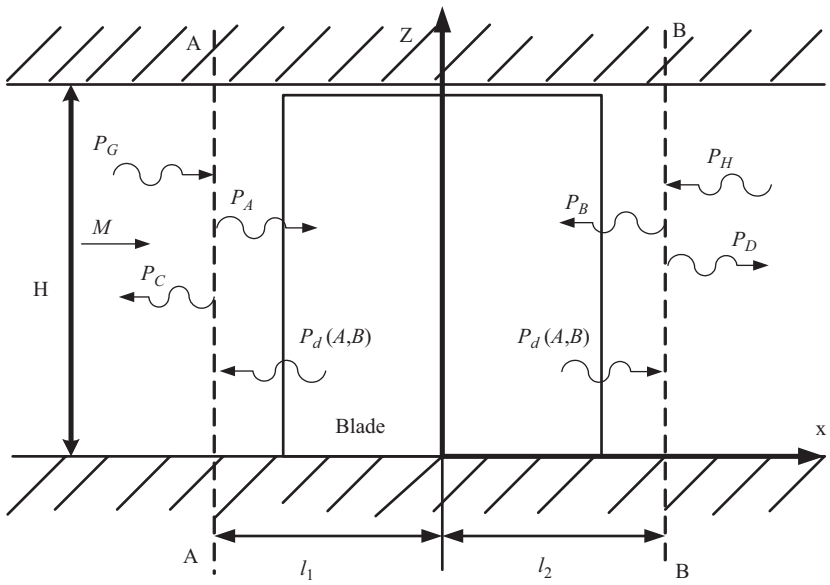

Fig. 4. The blade row section model in an infinite duct.

has shown that

$$p(\vec{x},t)=\int_{-T}^{T}\mathrm{d}\tau\int_{A}\left[G\left(\frac{\partial}{\partial n}+\frac{V_n}{a_0^2}\frac{D_0}{D\tau}\right)p(\vec{y},\tau)-p(\vec{y},\tau)\left(\frac{\partial}{\partial n}+\frac{V_n}{a_0^2}\frac{D_0}{D\tau}\right)G(\vec{y},\tau\big|\vec{x},t)\right]\mathrm{d}S(\vec{y}). \tag{5}$$

With the same boundary condition as Eq. (3) described, Sun and Kaji [17] has shown that the outgoing-wave solution may be written as

$$\bar{p}(\xi,\eta,\zeta)=-\frac{\beta_r}{4\pi b^2 h}\int_A\int_{-\infty}^{+\infty}\Delta p(\xi_0,\zeta_0)\sum_{n=1}^{\infty}\left[\frac{\cos k_n\zeta\,\cos k_n\zeta_0}{\Lambda_0}\times\sum_{q=-\infty}^{q=\infty}\mathrm{sgn}(\eta-qh_2\beta_r)\mathrm{e}^{\mathrm{i}q\sigma-\mathrm{i}(\alpha-k_bM_r)[\xi-(\xi_0+qh_1)]-\mathrm{i}\sqrt{k_b^2-\alpha^2-k_n^2}|\eta-qh_2\beta_r|}\right]\mathrm{d}\alpha\,\mathrm{d}S, \tag{6}$$

where $\Delta p(\xi_0,\zeta_0,\tau)$ is pressure difference between the lower and upper surface of a blade, q is the blade number, and for expedience the term correlative with time in the function is omitted. The coordinate transforms $\xi=x/b$, $\eta=y\beta_r/b$, $\zeta=z\beta_r/b$ are introduced here. And where

$$k_b=\frac{\omega_b b}{a_0\beta_r^2}, \tag{7}$$

$$\beta_r=\sqrt{1-M_r^2}, \tag{8}$$

$$k_n=\frac{\pi(n-1)}{h}=\frac{\pi(n-1)b}{H\beta_r},\quad n=1,2,3,\ldots, \tag{9}$$

$$\Lambda_0=\begin{cases}1 & n=1,\\ 0.5 & n\neq 1.\end{cases} \tag{10}$$

2.2.1. The upwash integral equation

By letting $\eta\to 0$, the corresponding upwash integral equation for the pressure across the 0th blade in terms of the known upwash velocity for the zeroth stator blade can therefore be written as

$$\frac{\bar{v}(\xi,0,\zeta)}{U_r}=\int_0^1\int_{-1}^{1}f(\xi_0,\zeta_0)K_0(\xi-\xi_0,\zeta\big|\zeta_0)\,\mathrm{d}\xi_0\,\mathrm{d}\zeta_0, \tag{11}$$

where

$$f(\xi_0,\zeta_0)=\frac{\Delta\bar{p}_0(\xi_0,\zeta_0)}{\rho_0U_r^2}, \tag{12}$$

$$K_0(\xi-\xi_0,\zeta\big|\zeta_0)=\frac{i\beta_r}{4\pi}\lim_{\eta\to 0}\frac{\partial}{\partial\eta}\int_{-\infty}^{+\infty}\sum_{n=1}^{+\infty}\left[\frac{\cos(k_n\zeta)\,\cos(k_n\zeta_0)\mathrm{e}^{-\mathrm{i}(\alpha-k_bM_r)(\xi-\zeta_0)}}{\Lambda_0\left(\alpha-\dfrac{k_b}{M_r}\right)}\times\frac{1}{2i}\left(\frac{\mathrm{e}^{\mathrm{i}\sqrt{k_b^2-\alpha^2-k_n^2}\eta}\mathrm{e}^{\frac{\mathrm{i}}{2}\Delta_-}}{\sin\frac{1}{2}\Delta_-}+\frac{\mathrm{e}^{-\mathrm{i}\sqrt{k_b^2-\alpha^2-k_n^2}\eta}\mathrm{e}^{\frac{\mathrm{i}}{2}\Delta_+}}{\sin\frac{1}{2}\Delta_+}\right)\right]\mathrm{d}\alpha, \tag{13}$$

$$\Delta_-=(\Gamma+h_1\alpha)+h_2\beta_r\beta^-, \tag{14}$$

$$\Delta_+=(\Gamma+h_1\alpha)+h_2\beta_r\beta^+, \tag{15}$$

$$\Gamma = \sigma - k_b M_r h_1. \tag{16}$$

As the integrand in Eq. (13) possesses only poles at $\alpha_v = K_b/M_r$ and at the points where $\Delta_\pm = 2m\pi$ for $m = 0, \pm 1, \pm 2, \ldots$. It follows from Eqs. (14) and (15) that the points are determined by

$$\alpha^{\pm}_{m,n} = -\frac{\Gamma_m h_1}{d^2} \pm \frac{\beta_r h_2}{d}\sqrt{k_b^2 - k_n^2 - \left(\frac{\Gamma_m}{d}\right)^2}, \tag{17}$$

where

$$\Gamma_m = \Gamma - 2m\pi \quad (m = 0, \pm 1, \pm 2, \ldots,), \tag{18}$$

$$d = \sqrt{h_1^2 + h_2^2\beta_r^2}. \tag{19}$$

Due to different α, the kernel function will be different. Hence, for the downstream pressure wave $(\xi - \xi_0) > 0$, the kernel function is

$$\begin{aligned} K_0(\xi - \xi_0, \zeta|\zeta_0) = {} & \frac{\beta_r^2 h_2}{2d^2}\sum_{m=-\infty}^{+\infty}\sum_{n=1}^{+\infty}\frac{\cos k_n\zeta \cos k_n\zeta_0}{\Lambda_0} \\ & \times \frac{(k_b^2 - \alpha_{m,n}^{+2} - k_n^2)\mathrm{e}^{-\mathrm{i}(\alpha^+_{m,n} - k_b M_r)(\xi - \xi_0)}}{(\alpha^+_{m,n} + \Gamma_m h_1/d^2)(\alpha^+_{m,n} - k_b/M_r)} \\ & + \frac{\beta_r}{2}\sum_{n=1}^{+\infty}\frac{\cos k_{nv}\zeta \cos k_{nv}\zeta_0}{\Lambda_v} \times \frac{\beta_v \sin(h_2\beta_r\beta_v)\mathrm{e}^{-\mathrm{i}(\beta_r^2 K_b/M_r)(\xi - \xi_0)}}{\cos(h_2\beta_r\beta_v) - \cos(\Gamma + \alpha_v h_1)}, \end{aligned} \tag{20}$$

where α_v, β_v are the wavenumber of vortex wave propagating downstream, i.e.

$$\alpha_v = \frac{k_b}{M_r}, \tag{21}$$

$$\beta_v = \sqrt{k_b^2 - \alpha_v^2 - k_{nv}^2}. \tag{22}$$

For the upstream pressure wave $(\xi - \xi_0) < 0$, the kernel function is

$$\begin{aligned} K_0(\xi - \xi_0, \zeta|\zeta_0) = {} & -\frac{\beta_r^2 h_2}{2d^2}\sum_{m=-\infty}^{+\infty}\sum_{n=1}^{+\infty}\frac{\cos k_n\zeta \cos k_n\zeta_0}{\Lambda_0} \\ & \times \frac{(k_b^2 - \alpha_m^{-2} - k_q^2)\mathrm{e}^{-\mathrm{i}(\alpha^-_m - k_b M_r)(\xi - \xi_0)}}{(\alpha^-_{m,n} + \Gamma_m h_1/d^2)(\alpha^-_{m,n} - k_b/M_r)}. \end{aligned} \tag{23}$$

2.2.2. The outgoing acoustic wave

By letting $\eta \to 0$, the corresponding outgoing acoustic wave solution for the pressure across the 0th blade in terms of the known force $f(\xi_0, \zeta_0)$ on the blade face may be written as

$$p_{\mathrm{out}}(\xi, \eta, \zeta) = \int_0^1\int_{-1}^1 f(\xi_0, \zeta_0)K_p(\xi - \xi_0, \eta, \zeta|\zeta_0)\,\mathrm{d}\xi_0\,\mathrm{d}\zeta_0, \tag{24}$$

where

$$\begin{aligned} K_p(\xi - \xi_0, \eta, \zeta|\zeta_0) = {} & -\frac{\rho_0 U_r^2}{4\pi}\int_{-\infty}^{+\infty}\sum_{n=1}^{+\infty}\frac{\cos k_n\zeta \cos k_n\zeta_0 \mathrm{e}^{-\mathrm{i}(\alpha - k_b M_r)(\xi - \xi_0)}}{\Lambda_0} \\ & \times \frac{1}{2\mathrm{i}}\left[\frac{\mathrm{e}^{\mathrm{i}\sqrt{k_b^2 - \alpha^2 - k_n^2}\eta}\mathrm{e}^{\frac{1}{2}\Delta_-}}{\sin\frac{1}{2}\Delta_-} + \frac{\mathrm{e}^{-\mathrm{i}\sqrt{k_b^2 - \alpha^2 - k_n^2}\eta}\mathrm{e}^{\frac{1}{2}\Delta_+}}{\sin\frac{1}{2}\Delta_+}\right]\mathrm{d}\alpha. \end{aligned} \tag{25}$$

For the downstream pressure wave $(\xi-\xi_0)>0$, the kernel function is

$$K_p^+(\xi-\xi_0,\eta,\zeta|\zeta_0)=\frac{\rho_0 U_r^2\beta_r^2 h_2}{2d^2}\sum_{m=-\infty}^{+\infty}\sum_{n=1}^{+\infty}\frac{\cos k_n\zeta\,\cos k_n\zeta_0}{\Lambda_0}\times\frac{\left(-\sqrt{k_b^2-\alpha_{m,n}^{+2}-k_n^2}\right)e^{-i(\alpha_m^+-k_bM_r)(\xi-\xi_0)-i\sqrt{k_b^2-\alpha_{m,n}^{+2}-k_q^2}\eta}}{(\alpha_{m,n}^+ + \Gamma_m h_1/d^2)}. \tag{26}$$

For the upstream pressure wave $(\xi-\xi_0)<0$, the kernel function is

$$K_p^-(\xi-\xi_0,\eta,\zeta|\zeta_0)=-\frac{\rho_0 U_r^2\beta_r^2 h_2}{2d^2}\sum_{m=-\infty}^{+\infty}\sum_{n=1}^{+\infty}\frac{\cos k_n\zeta\,\cos k_n\zeta_0}{\Lambda_0}\times\frac{\sqrt{k_b^2-\alpha_{m,n}^{-2}-k_n^2}e^{-i(\alpha_{m,n}^--k_bM_r)(\xi-\xi_0)+i\sqrt{k_b^2-\alpha_{m,n}^{-2}-k_q^2}\eta}}{(\alpha_{m,n}^- + \Gamma_m h_1/d^2)}. \tag{27}$$

2.2.3. *A solution in a finite domain for the blade row*

The above solution only exists for an infinitely long duct. So, we try to solve the sound field for a finite domain from $x=-l_1$ to l_2 as shown in Fig. 4. It is noted that the acoustic pressure p in the domain can be regarded as a sum of an undisturbed incident acoustic pressure component p_i and a disturbance pressure component p_d, i.e.

$$p=p_i+p_d. \tag{28}$$

For simplicity, in most of the computational models, the incident acoustic wave p_i is usually treated as a single mode coming from one direction, which interacts directly with the scattering object. However, superposition principle for a liner system states that a linear combination of solution to a linear equation is again a solution of the linear system, so, we can directly consider the incident waves interacting with the blade row shown in Fig. 4 with the following expression:

$$p_i=p_A+p_B=\sum_{\mu=1}^{N}\Big[A_\mu\cos(k_\mu\zeta)e^{-i\beta_{m,\mu}^+\eta-i(\alpha_{m,\mu}^+-k_bM_r)(\xi+L_1)} + B_\mu\cos(k_\mu\zeta)e^{-i\beta_{m,\mu}^-\eta-i(\alpha_{m,\mu}^--k_bM_r)(\xi-L_2)}\Big], \tag{29}$$

where

$$\beta^\pm=\pm\sqrt{k_b^2-\alpha^2-k_\mu^2}. \tag{30}$$

Using momentum equation and Eq. (29) one can obtain expressions for the acoustic fluid velocity of sub-incident waves, the η component of which is given by

$$\begin{aligned}v_i'(\xi,\eta,\zeta)&=-\frac{\beta_r}{\rho_0 U_r}e^{-i\frac{k_b\beta_r^2}{M_r}\xi}\int_{-\infty}^{\xi}\frac{\partial p_i}{\partial\eta}e^{i\frac{k_b\beta_r^2}{M_r}\xi'}\,d\xi'\\&=\sum_{\mu=1}^{+\infty}\left(\frac{-A_\mu\beta_r\beta_{m,\mu}^+\cos(k_\mu\zeta)e^{-i\beta_{m,\mu}^+\eta-i(\alpha_{m,\mu}^+-k_bM_r)(\xi+L_1)}}{\rho_0 U_r\left(\alpha_{m,\mu}^+-\frac{k_b}{M_r}\right)}\right.\\&\quad\left.+\frac{-B_\mu\beta_r\beta_{m,\mu}^-\cos(k_\mu\zeta)e^{-i\beta_{m,\mu}^-\eta-i(\alpha_{m,\mu}^--k_bM_r)(\xi-L_2)}}{\rho_0 U_r\left(\alpha_{m,\mu}^--\frac{k_b}{M_r}\right)}\right).\end{aligned} \tag{31}$$

As there must be no net upwash at the blade surface [9], the perturbation velocity of blade may be given by

$$v_b = v_i'. \tag{32}$$

Substituting Eq. (31) into the integral Eq. (11), the integral equation can be reduced to a set of algebraic equation for the unknown $f_{A_\mu}(\xi_0,\zeta_0)$ and $f_{B_\mu}(\xi_0,\zeta_0)$, which are defined as modal pressure coefficient related to Eq. (12). Then using the outgoing wave equation (24), the outgoing acoustic wave pressure p_{out} can be obtained as

$$p_{\text{out}}(\xi,\eta,\zeta) = \int_0^1 \int_{-1}^1 \left(\sum_{\mu=1}^{\infty} A_\mu f_{A_\mu}(\xi_0,\zeta_0) + B_\mu f_{B_\mu}(\xi_0,\zeta_0) \right) \times K_p(\xi-\xi_0,\eta,\zeta|\zeta_0)\,\mathrm{d}\xi_0\,\mathrm{d}\zeta_0. \tag{33}$$

By letting [18]

$$\zeta_{0j} = \frac{j}{M_0}, \quad j = 0,1,2,\ldots,M_0-1, \tag{34}$$

$$\psi_{0k} = \frac{k\pi}{N_0}, \quad k = 1,2,\ldots,N_0, \tag{35}$$

$$\xi_{0k} = \cos\psi_{0k}. \tag{36}$$

Eq. (33) can be expressed as

$$p_{\text{out}} = \sum_{n=1}^{+\infty} \frac{(-\beta_{m,n}^{\pm})\cos k_n\zeta \mathrm{e}^{-\mathrm{i}(\alpha_{m,n}^{\pm}-k_bM_r)\xi+\mathrm{i}\beta_{m,n}^{\pm}\eta}}{\Lambda_0\left(\alpha_{m,n}^{\pm}+\dfrac{\Gamma_m h_1}{d^2}\right)}(A_\mu F_{n\pm}^{A_\mu} + B_\mu F_{n\pm}^{B_\mu}), \tag{37}$$

where

$$F_{n\pm}^{A_\mu} = \frac{\pm\beta_r h_2\pi}{2d^2(M_0\times N_0)}\left(\sum_{j=0}^{M_0-1}\sum_{k=1}^{N_0} f_{A_\mu}(\xi_{0k},\zeta_{0j})\right)\cos k_n\zeta_{0j}\mathrm{e}^{\mathrm{i}(\alpha_{m,n}^{-}-k_bM_r)\xi_{0k}}, \tag{38}$$

$$F_{n\pm}^{B_\mu} = \frac{\pm\beta_r h_2\pi}{2d^2(M_0\times N_0)}\left(\sum_{j=0}^{M_0-1}\sum_{k=1}^{N_0} f_{B_\mu}(\xi_{0k},\zeta_{0j})\right)\cos k_n\zeta_{0j}\mathrm{e}^{\mathrm{i}(\alpha_{m,n}^{-}-k_bM_r)\xi_{0k}}. \tag{39}$$

For matching with other elements appropriately, as seen in Fig. 3, a transform of coordinate is used here, i.e.

$$\begin{cases} x' = \xi b\cos\theta - \dfrac{\eta b}{\beta_r}\sin\theta, \\ y' = \dfrac{\eta b}{\beta_r}\cos\theta + \xi b\sin\theta, \\ z' = \dfrac{\varsigma b}{\beta_r}. \end{cases} \tag{40}$$

By transforming the coordinate system, one obtains the wavenumber α,β

$$\alpha'^{\pm}_{m,n} = -\frac{\beta_r\beta_{m,n}^{\pm}\sin\theta}{b} + \frac{(\alpha_{m,n}^{\pm}-k_bM_r)\cos\theta}{b}, \tag{41}$$

$$\beta'^{\pm}_{m} = \frac{\beta_r\beta_{m,n}^{\pm}\cos\theta}{b} + \frac{(\alpha_{m,n}^{\pm}-k_bM_r)\sin\theta}{b}. \tag{42}$$

Using the same treatment as mentioned above, the x' component acoustic fluid velocity of disturbance pressure at the cross-section is given by

$$u(x,y,z) = -\alpha'^{\pm}_{m,n} p_{\text{out}}/\rho_0(\omega + U\alpha'^{\pm}_{m,n} + V\beta'^{\pm}_{m}). \tag{43}$$

As a specific example, we can use the present method to construct a close matrix equation to obtain the solution for an infinitely long duct described in Fig. 4. In this case, an incident wave p_H impinges upon the cascade from the downstream. In fact, with the interface $x = -l_1$ or l_2 as a relative coordinate, the sound propagation in a different direction can be described as

$$p_A = \sum_{n=1}^{N} A_n \cos(k_n\zeta)\mathrm{e}^{-\mathrm{i}\beta'^{+}_{m,n}y' - i\alpha'^{+}_{m,n}(x'+l_1)}, \tag{44}$$

$$p_B = \sum_{n=1}^{N} B_n \cos(k_n\zeta)\mathrm{e}^{-\mathrm{i}\beta'^{-}_{m,n}y' - i\alpha'^{-}_{m,n}(x'-l_2)}, \tag{45}$$

$$p_C = \sum_{n=1}^{N} C_n \cos(k_n\zeta)\mathrm{e}^{-\mathrm{i}\beta'^{-}_{m,n}y' - i\alpha'^{-}_{m,n}(x'+l_1)}, \tag{46}$$

$$p_D = \sum_{n=1}^{N} D_n \cos(k_n\zeta)\mathrm{e}^{-\mathrm{i}\beta'^{+}_{m,n}y' - i\alpha'^{+}_{m,n}(x'-l_2)}, \tag{47}$$

$$p_H = \sum_{n=1}^{N} H_n \cos(k_n\zeta)\mathrm{e}^{-\mathrm{i}\beta'^{-}_{m,n}y' - i\alpha'^{-}_{m,n}(x'-l_2)}. \tag{48}$$

All these waves are composed of modal components that can be specified by the notation (m,n). In addition, the known source p_H is assumed to be located at $x = +\infty$, and only cut-on modes are considered. On the other hand, once the unknown coefficients p_A, p_B, p_C, p_D $(n = 1,2,3,\ldots,N)$ are determined, the corresponding acoustic field in the duct can be obtained through Eqs. (44)–(48). Eqs. (37) and (44)–(48) imply that, to describe the sound field in the duct, $4N$ unknown coefficients (A_n, B_n, C_n, D_n) have to be determined. According to the pressure and axial velocity continuity conditions on the cross-section C–C and D–D

$$\begin{aligned} p_C^- &= p_C^+, \quad u_C^- = u_C^+, \\ p_D^- &= p_D^+, \quad u_D^- = u_D^+. \end{aligned} \tag{49}$$

Using the orthogonality of eigenfunctions, one can obtain $4N$ algebraic equations for the unknown coefficients. The set of equations is reduced into

$$\begin{Bmatrix} ss_C^1 & ss_A^1 & ss_B^1 & 0 \\ ss_C^2 & ss_A^2 & ss_B^2 & 0 \\ 0 & ss_A^3 & ss_B^3 & ss_D^3 \\ 0 & ss_A^4 & ss_B^4 & ss_D^4 \end{Bmatrix} \begin{pmatrix} p_C \\ p_A \\ p_B \\ p_D \end{pmatrix} = \begin{pmatrix} 0 \\ 0 \\ p_H \\ u_H \end{pmatrix}, \tag{50}$$

where each ss denotes a coefficients matrix, for example,

$$ss_A^1 = \begin{bmatrix} -1 & 0 & 0 & 0 \\ 0 & -1 & 0 & 0 \\ 0 & 0 & -1 & 0 \\ 0 & 0 & 0 & -1 \end{bmatrix} + \begin{bmatrix} -cs_{1-}^{A_1} & -cs_{1-}^{A_2} & \cdots & -cs_{1-}^{A_N} \\ -cs_{2-}^{A_1} & -cs_{2-}^{A_2} & \cdots & -cs_{2-}^{A_N} \\ \vdots & \vdots & \ddots & \vdots \\ -cs_{N-}^{A_1} & -cs_{N-}^{A_2} & \cdots & -cs_{N-}^{A_N} \end{bmatrix}, \tag{51}$$

where

$$cs_{n-}^{A_\mu} = \frac{(-\beta_{m,n}^{-})\mathrm{e}^{-\mathrm{i}\alpha'^{-}_{m,n}x' - i\beta'^{-}_{m}y'}}{\Lambda_0\left(\alpha_{m,n}^{-} + \dfrac{\Gamma_m h_1}{d^2}\right)} F_{n-}^{A_\mu}, \tag{52}$$

$$p_H = \overbrace{\{H_1, H_2, \cdots, H_n\}}^{N}, \tag{53}$$

$$u_H = \overbrace{\left\{\frac{\alpha'^{-}_{m,1}H_1}{\rho_0(\omega + U\alpha'^{-}_{m,1} + V\beta'^{-}_{m,1})}, \frac{\alpha'^{-}_{m,2}H_2}{\rho_0(\omega + U\alpha'^{-}_{m,2} + V\beta'^{-}_{m,2})}, \cdots \frac{\alpha_{m,n}^{-}H_n}{\rho_0(\omega + U\alpha_{m,n}^{-} + V\beta_{m,n}^{-})}\right\}}^{N}. \tag{54}$$

And $\{ss^1{}_A\}_{N\times N}$ represents a matrix related to the sound wave p_A defined in Eq. (44). Therefore, for each section, the corresponding matrix can be described as

$$\begin{Bmatrix} ss_A^1 & ss_B^1 \\ ss_A^2 & ss_B^2 \\ ss_A^3 & ss_B^3 \\ ss_A^4 & ss_B^4 \end{Bmatrix}. \tag{55}$$

Up to now, we have derived the solution in a finite domain with the unknown variables on the interfaces. For simplicity, the solution consisting of Eqs. (28), (29), (37) and the corresponding matrix expression defined in Eq. (55) is called as a "transfer element". For convenience in the following discussions, we call what is suggested in this investigation as "transfer element method" (shorten by TEM).

2.3. Formulation for the acoustic lining section

As is shown in Fig. 5, a duct of arbitrary uniform cross-section is considered here, in which a uniform mean flow is contained. The incident waves interacting with the liner is similar as that of the blade row section with

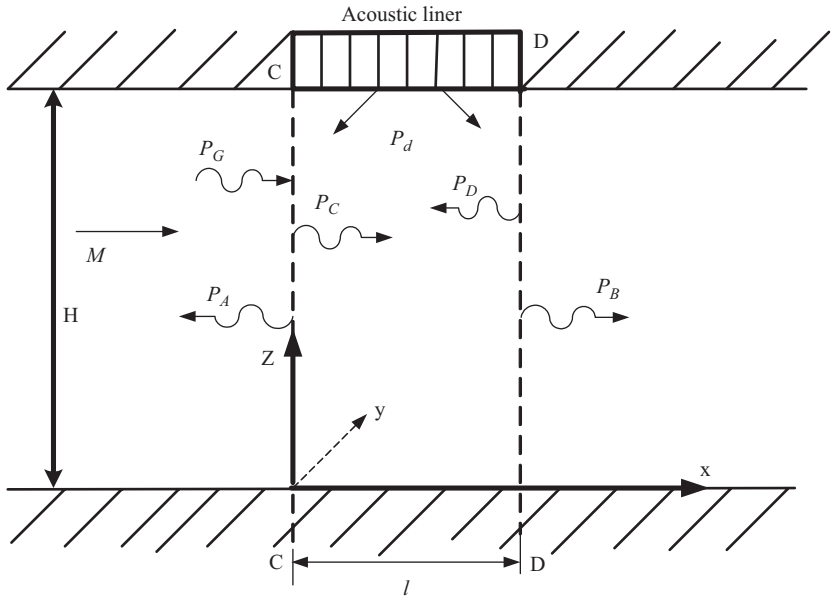

Fig. 5. The liner section model in an infinite duct.

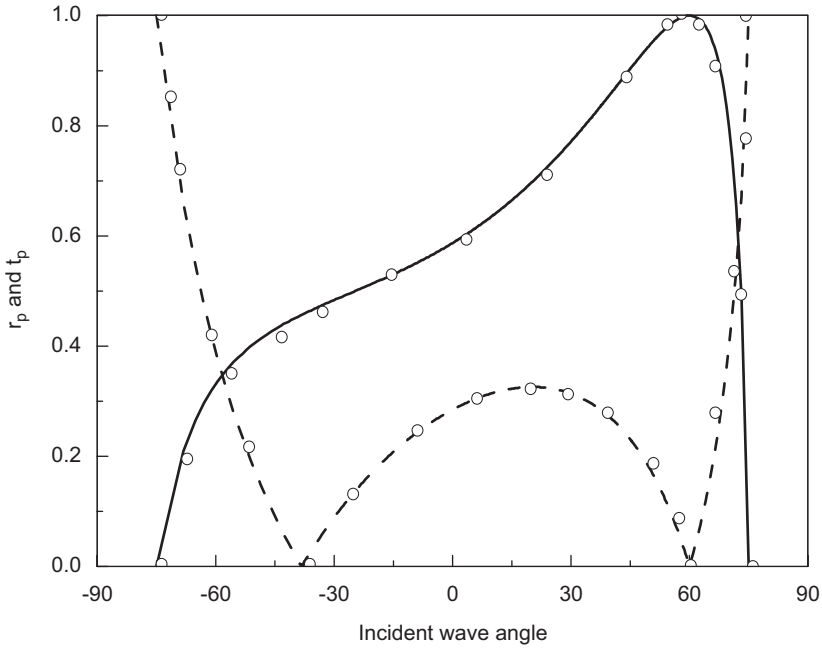

Fig. 6. Comparison with Kaji and Okazaki's numerical results. — Transmission coefficient, – – reflection coefficient, ○ Ref. [18], Stagger angle of cascade: $\theta = 60^\circ$, $M_r = 0.5$, $\lambda = 1.57$, $s/c = 1$.

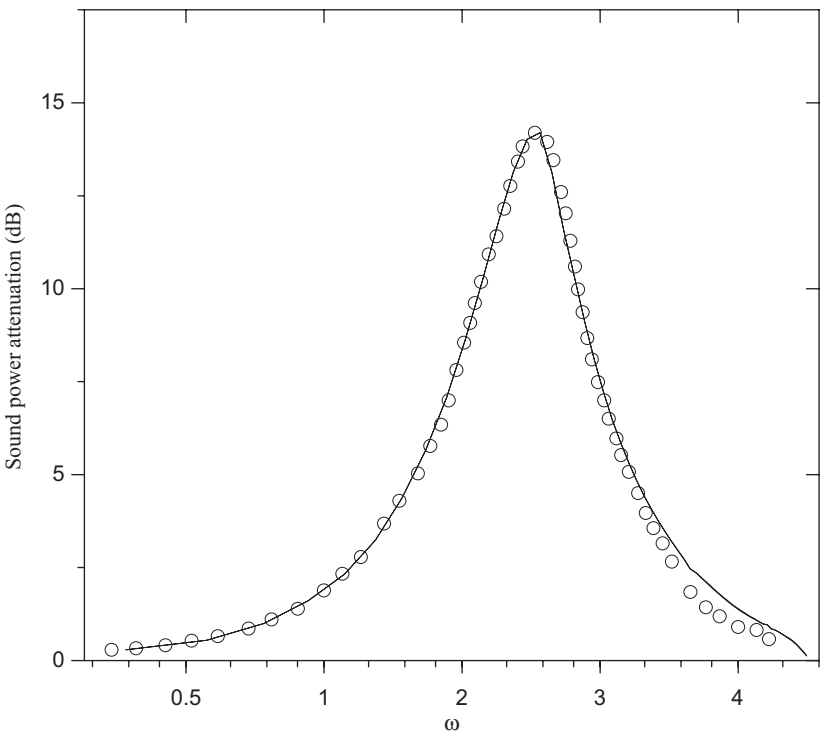

Fig. 7. Comparison with Namba's numerical results [18]. Sound power attenuation for the fundamental (0,0) mode incident and a uniform liner. — present result, ○ Ref. [18], Ma = 0, $l = 4.339$, $d = 0.271$, $R = 1.4$, $\omega_0 = 25.57$.

the following expression:

$$p_i = p_C + p_D = \sum_{\mu=1}^{N} \left[C_\mu \Phi_{m,\mu}(y,z) \mathrm{e}^{\mathrm{i}\gamma^+_{m\mu} x} + D_\mu \Phi_{m,\mu}(y,z) \mathrm{e}^{\mathrm{i}\gamma^-_{m\mu}(x-l)} \right], \tag{56}$$

where C_μ and D_μ are unknown coefficients, and

$$\Phi_{m,n}(y,z) = \sqrt{\varepsilon_n} \cos\left(n\pi \frac{z}{H}\right), \tag{57}$$

$$\varepsilon_n = \begin{cases} 1 & n = 0, \\ 2 & n \neq 0, \end{cases} \tag{58}$$

$$\begin{cases} \gamma^-_{m,n} = \dfrac{Mk_0}{\beta_a^2} + \dfrac{\kappa_{n,m}}{\beta_a^2} & \text{(upstream)}, \\ \gamma^+_{m,n} = \dfrac{Mk_0}{\beta_a^2} - \dfrac{\kappa_{n,m}}{\beta_a^2} & \text{(downstream)}, \end{cases} \tag{59}$$

$$\kappa_{n,m} = \begin{cases} \sqrt{k_0^2 - \beta_a^2 k_{m,n}^2} & k_0^2 > \beta_a^2 k_{m,n}^2, \\ -i\sqrt{\beta_a^2 k_{m,n}^2 - k_0^2} & k_0^2 < \beta_a^2 k_{m,n}^2, \end{cases} \tag{60}$$

$$\beta_a^2 = \sqrt{1 - M^2}, \tag{61}$$

where $k_{m,n}$ denotes the eigenvalue due to the condition of solid wall.

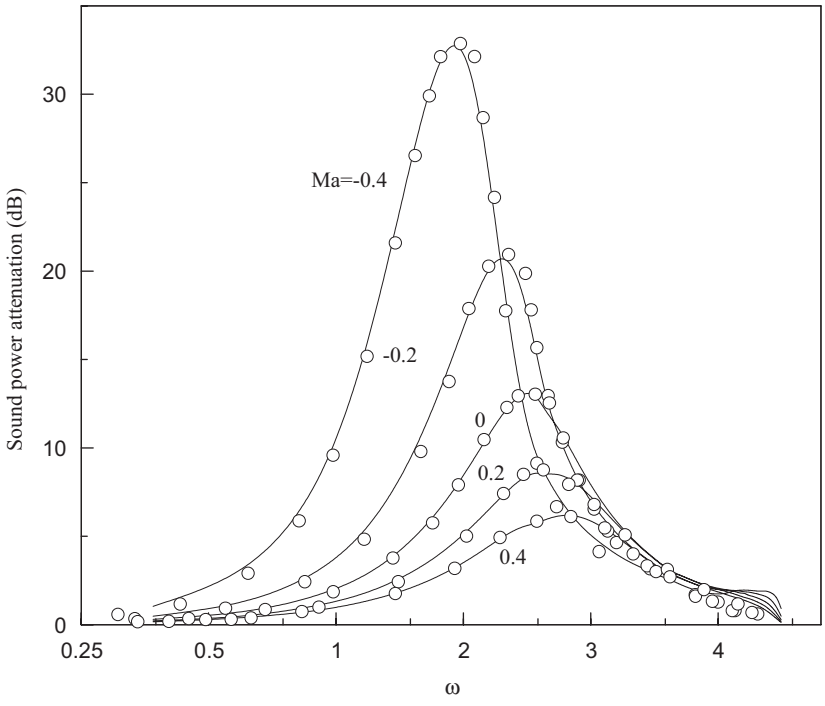

Fig. 8. Comparison with Ref. [18]. Sound power attenuation for the fundamental (0,0) mode incident wave under different Mach number mean flow. — Present result, ○ Ref. [18], $l = 4.339$, $d = 0.271$, $R = 1.4$, $\omega_0 = 25.57$.

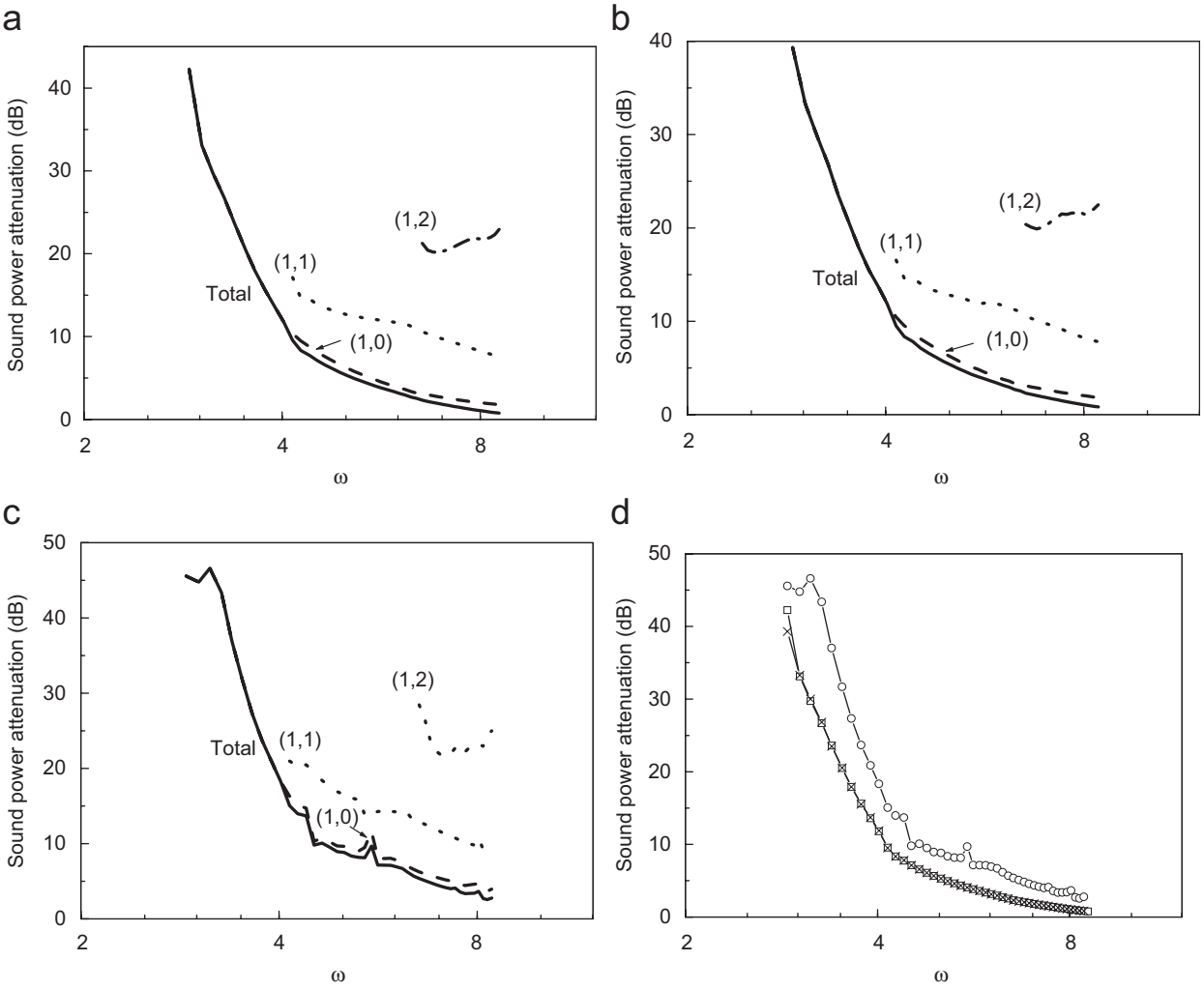

Fig. 9. (a) Modal spectra of the sound attenuation of the liner for the (1,0) mode incident from upstream side. (b) Effect of the cascade on the sound attenuation of the liner. (c) Modal spectra of the sound attenuation of the combination of the liner and the cascade. (d) The comparison of the total sound attenuation in (a)–(c), –□– total sound attenuation of case (a), – × – total sound attenuation of case (b), –○– total sound attenuation of case (c). $M_r = 0.4$, $l = 4.339$, $s/c = 1.0$, (1,0), (1,1) and (1,2) in (a)–(c) represent the cut-on modes corresponding to the given frequency.

On the other hand, from Eq. (4), the solution for the monopole source in this section will be eventually expressed as

$$p_d = \sum_{n=1}^{N} p_{dn}\Phi_{m,n}(y,z) = \frac{\rho_0}{2}\sum_{n=1}^{N}\frac{\Phi_{m,n}(y,z)e^{i\gamma_{m,n}^{\pm}x}}{\Gamma_{m,n}}\left\{\sum_{\mu=1}^{\infty}\left[C_\mu Q_{n\pm}^{C_\mu} + D_\mu Q_{n\pm}^{D_\mu}\right]\right\}, \tag{62}$$

where

$$Q_{n\pm}^{C_\mu} = \Phi_{m,\mu}(y,z)\sum_{k=1}^{\infty}\sum_{j=1}^{\infty}\Re_{jk,\mu,B_\mu}^{-1} I_j^{C_\mu} S_k^{n\pm}, \tag{63}$$

$$Q_{n\pm}^{D_\mu} = \Phi_{m,\mu}(y,z)\sum_{k=1}^{\infty}\sum_{j=1}^{\infty}\Re_{jk,\mu,C_\mu}^{-1} I_j^{D_\mu} S_k^{n\pm}, \tag{64}$$

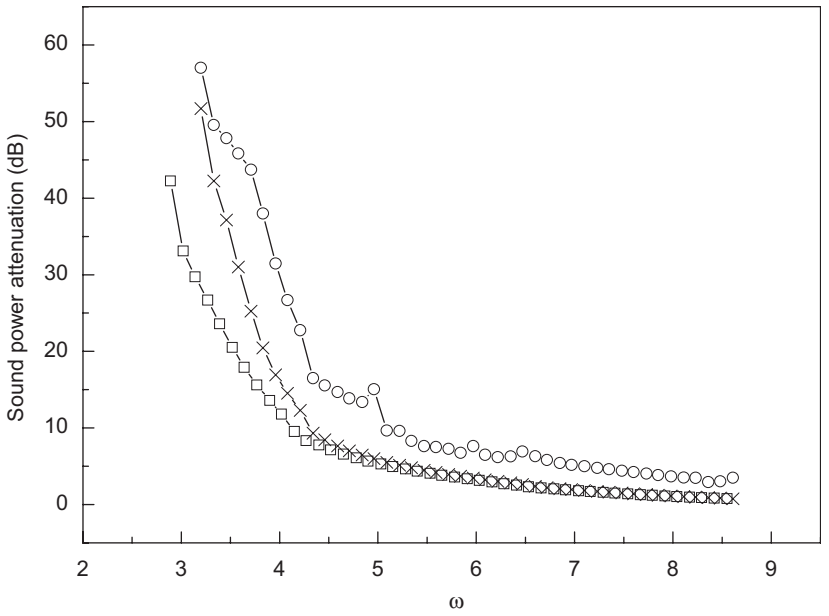

Fig. 10. The comparison of the total sound attenuation, –□– total sound attenuation of the case with liner only, – × – total sound attenuation of the liner with the effect of the cascade, –○– total sound attenuation of the case with both the liner and the cascade. $M_r = 0.4$, $l = 4.339$, $s/c = 0.9$.

$$S_k^{n\pm} = \int_s \Phi^*_{m,n}(y_0, z_0) \frac{[\omega + U\gamma^{\pm}_{m,n}]}{\kappa_{n,m}} \mathrm{e}^{-\mathrm{i}\gamma^{\pm}_{m,n}x_0} \left(1 + \frac{U}{\mathrm{i}\omega}\frac{\partial}{\partial x_0}\right) \sin\frac{k\pi x_0}{l}\, \mathrm{d}s(\vec{r}_0), \tag{65}$$

$$\Gamma_{m,n} = h, \tag{66}$$

$$(z_{jk} + \delta_{jk}Z)^{-1} = \Re^{-1}_{jk}, \tag{67}$$

$$\begin{aligned} I_j &= \frac{2}{l}\int_0^l \sum_{\mu=1}^{N} \left[C_\mu \Phi_{m,\mu} \mathrm{e}^{\mathrm{i}\gamma^{+}_{m,\mu}x} + D_\mu \Phi_{m,\mu} \mathrm{e}^{\mathrm{i}\gamma^{-}_{m,\mu}(x-l)}\right] \sin\frac{j\pi x}{l}\, \mathrm{d}x \\ &= \sum_{\mu=1}^{N} \Phi_{m,\mu}(y,z)\left[C_\mu I_j^{C_\mu} + D_\mu I_j^{D_\mu}\right], \end{aligned} \tag{68}$$

$$\begin{aligned} z_{jk} = \frac{\rho_0}{l} &\sum_{m=-\infty}^{\infty}\sum_{n=1}^{\infty} \frac{\Phi_{m,n}(y,z)}{\Gamma_{m,n}} \\ &\int_0^l \int_{s(\tau)} \frac{[\omega + U\gamma^{\pm}_{m,n}]}{\kappa_{n,m}} \Phi^*_{m,n}(y_0,z_0) \mathrm{e}^{\mathrm{i}\gamma^{\pm}_{m,n}(x-x_0)} \left(1 + \frac{U}{\mathrm{i}\omega}\frac{\partial}{\partial x_0}\right) \sin\frac{k\pi x_0}{l}\, \mathrm{d}s(\vec{r}_0) \sin\frac{j\pi x}{l}\, \mathrm{d}x. \end{aligned} \tag{69}$$

All the incident waves, reflective waves and scattering waves are composed of modal components that can also be specified by the notation (m, n). To describe the sound field in the duct, $4N$ unknown coefficients

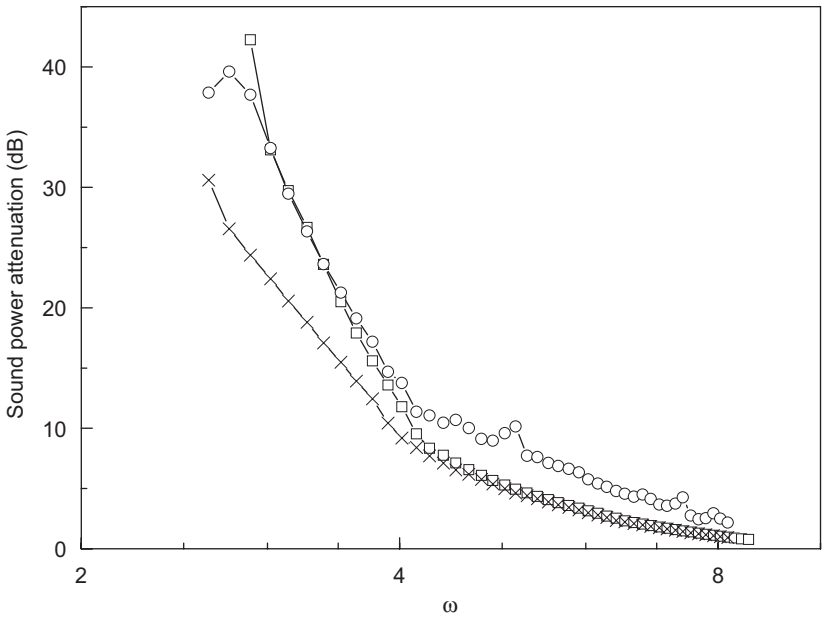

Fig. 11. The comparison of the total sound attenuation, –□– total sound attenuation of the case with liner only, – × – total sound attenuation of the liner with the effect of the cascade, –○– total sound attenuation of the case with both the liner and the cascade. $M_r = 0.4$, $l = 4.339$, $s/c = 1.1$.

$(A_\mu, B_\mu, C_\mu, D_\mu)$ have to be determined. Due to the pressure and axial velocity continuity condition on the cross-section A–A and B–B as mentioned in the blade row section, using the orthogonality of eigenfunction, one can also obtain $4N$ algebraic equations for the unknown coefficients. The set of equations is reduced to

$$\begin{Bmatrix} ss_A^1 & ss_C^1 & ss_D^1 & 0 \\ ss_A^2 & ss_C^2 & ss_D^2 & 0 \\ 0 & ss_C^3 & ss_D^3 & ss_B^3 \\ 0 & ss_C^4 & ss_D^4 & ss_B^4 \end{Bmatrix} \begin{pmatrix} p_A \\ p_C \\ p_D \\ p_B \end{pmatrix} = \begin{pmatrix} p_G \\ u_G \\ 0 \\ 0 \end{pmatrix}, \tag{70}$$

where each ss denotes a coefficients matrix, for example,

$$ss_c^1 = \begin{bmatrix} -1 & 0 & 0 & 0 \\ 0 & -1 & 0 & 0 \\ 0 & 0 & -1 & 0 \\ 0 & 0 & 0 & -1 \end{bmatrix} + \begin{bmatrix} -cs_{1-}^{C_1} & -cs_{1-}^{C_2} & \cdots & -cs_{1-}^{C_N} \\ -cs_{2-}^{C_1} & -cs_{2-}^{C_2} & \cdots & -cs_{2-}^{C_N} \\ \vdots & \vdots & \ddots & \vdots \\ -cs_{N-}^{C_1} & -cs_{N-}^{C_2} & \cdots & -cs_{N-}^{C_N} \end{bmatrix}, \tag{71}$$

where $cs_{n-}^{C_\mu} = (\rho_0/2)(e^{i\gamma_{m,n}^- x}/\Gamma_{m,n})Q_{n-}^{C_\mu}$, and

$$p_G = \overbrace{\{-G_1, -G_2, \ldots, -G_n\}}^{N}, \tag{72}$$

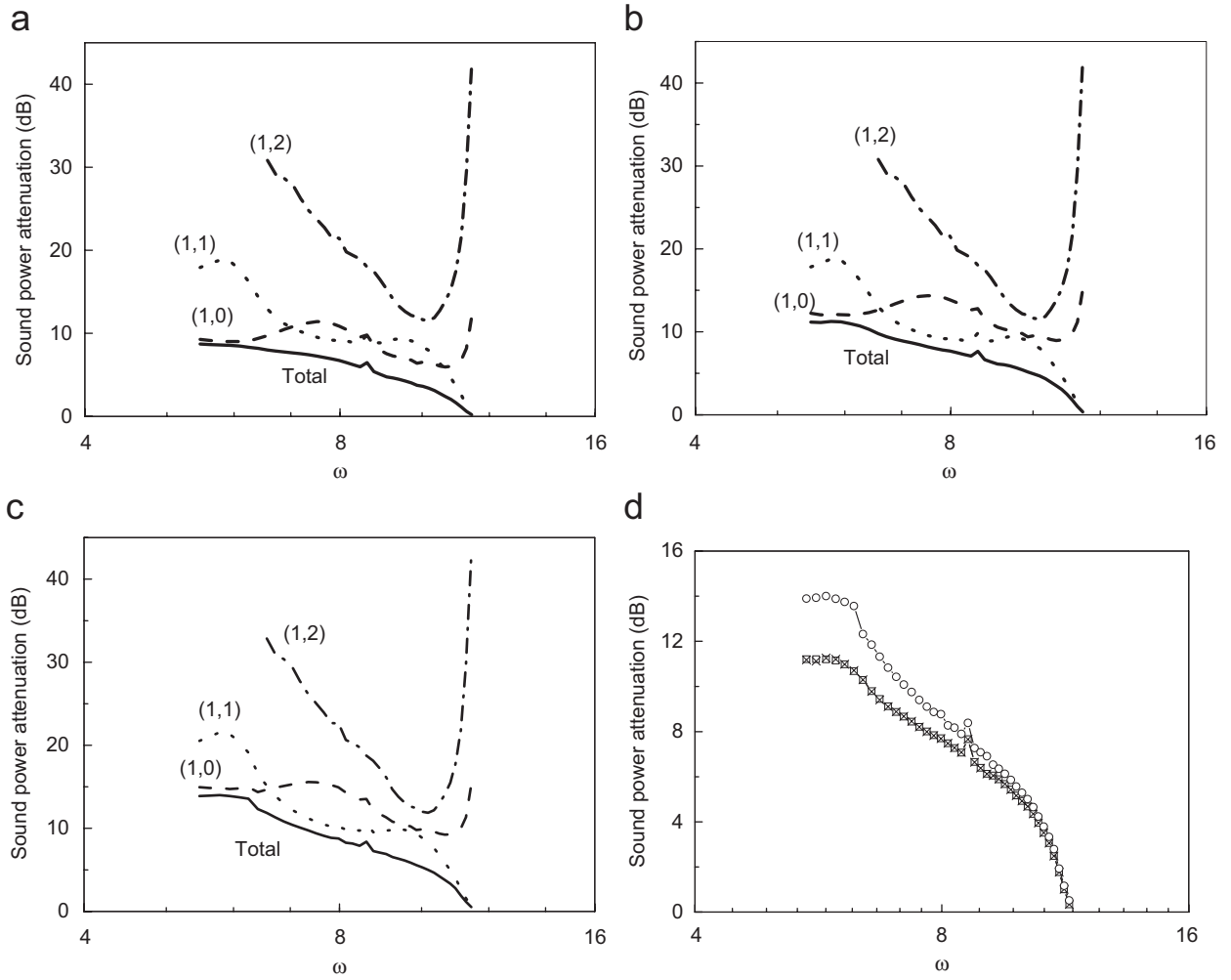

Fig. 12. (a) Modal spectra of the sound attenuation of the liner for the (1,1) mode incident from downstream side; (b) effect of a cascade on the sound attenuation of the liner; (c) modal spectra of the sound attenuation of the combination of the liner and the cascade; (d) the comparison of the total sound attenuation in (a)–(c), –□– total sound attenuation of case (a), – × – total sound attenuation of case (b), –○– total sound attenuation of case (c). $M_r = 0.4$, $l = 4.339$, $s/c = 1.0$, (1,0), (1,1) and (1,2) in (a)–(c) represent the cut-on modes corresponding to the given frequency.

$$u_G = \overbrace{\left\{ -\frac{\gamma^+_{m,1} G_1}{\omega + U\gamma^+_{m,1}}, -\frac{\gamma^+_{m,2} G_2}{\omega + U\gamma^+_{m,2}}, \cdots -\frac{\gamma^+_{m,n} G_n}{\omega + U\gamma^+_{m,n}} \right\}}^{N}. \tag{73}$$

And $\{ss^1{}_C\}_{N\times N}$ represents a matrix related to the sound wave p_C defined in Eq. (56). Therefore for each section, the corresponding matrix can be described as

$$\begin{Bmatrix} ss^1_C & ss^1_D \\ ss^2_C & ss^2_D \\ ss^3_C & ss^3_D \\ ss^4_C & ss^4_D \end{Bmatrix}. \tag{74}$$

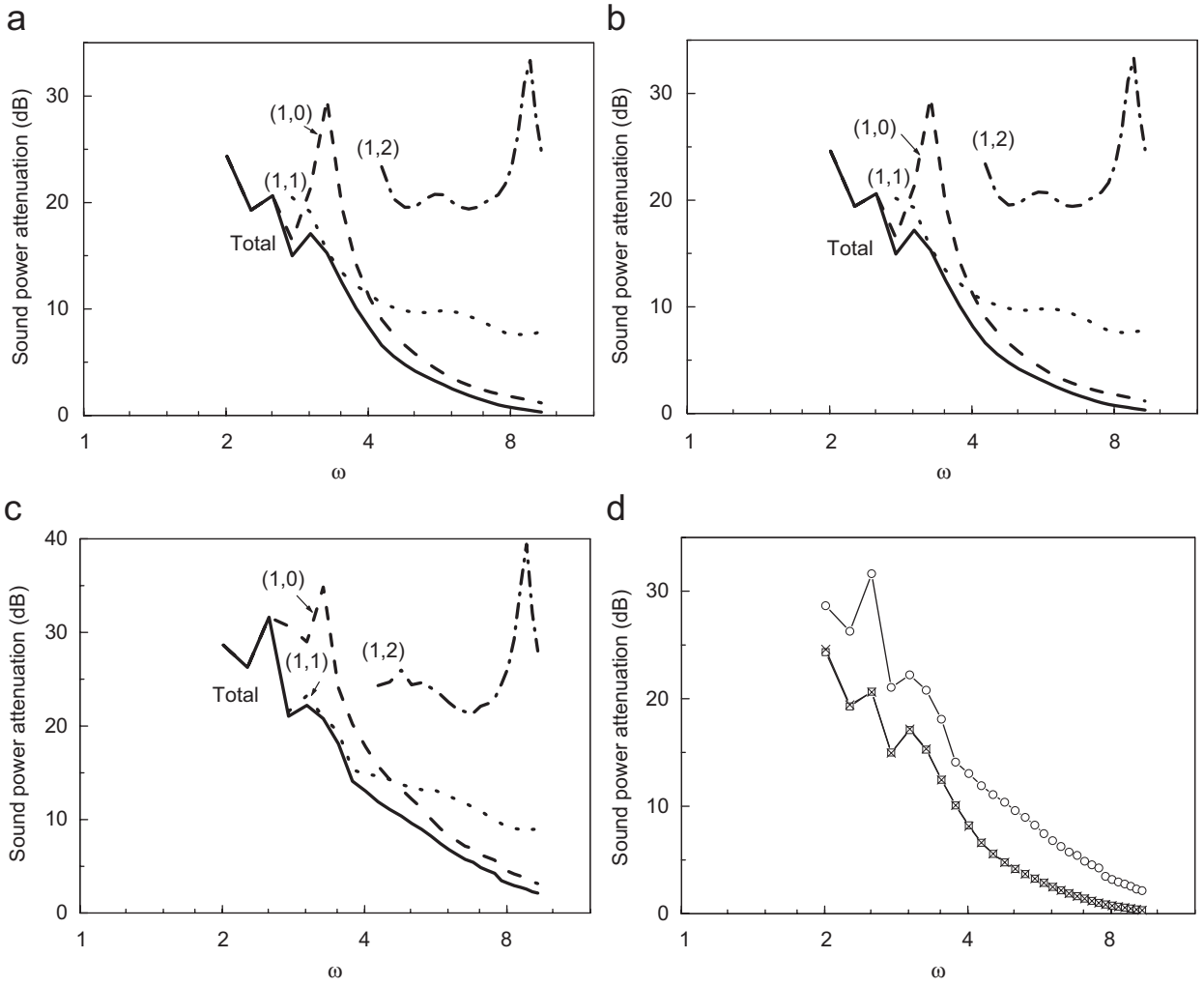

Fig. 13. (a) Modal spectra of the sound attenuation of the liner for the (1,0) mode incident from upstream side at high Mach number. (b) Effect of a cascade on the sound attenuation of the liner. (c) Modal spectra of the sound attenuation of the combination of the liner and the cascade. (d) The comparison of the total sound attenuation in (a)–(c), –□– total sound attenuation of case (a), – × – total sound attenuation of case (b), –○– total sound attenuation of case (c). $M_r = 0.8$, $l = 4.339$, $s/c = 1.0$, (1,0), (1,1) and (1,2) in (a)–(c) represent the cut-on modes corresponding to the given frequency.

Again, we have derived the solution in a finite domain with the unknown variables on the interfaces. Therefore, the "transfer element" of lined wall section is constructed.

2.4. The combination of the two sections

As shown in Fig. 2, the liner section and blade row section are combined into a new model. The solution for this new model can be obtained by combining the two transfer elements, and then establishing the relation between the transfer elements by imposing suitable conditions on the surface of each element. Using the TEM one can eventually obtain $6N$ algebraic equations for the $6N$ unknown coefficients (A_μ,B_μ,C_μ,D_μ,E_μ,F_μ). The known p_i or v_i will be included the right vector for a set of equations. Compared to the mode-matching method [19], the transfer element constructed here avoids calculating the difficult complex eigenvalues and the need to assume that the wall impedance is piecewise uniform. Moreover, the eigenfunctions still satisfy orthogonality, which means there is good convergence theoretically.

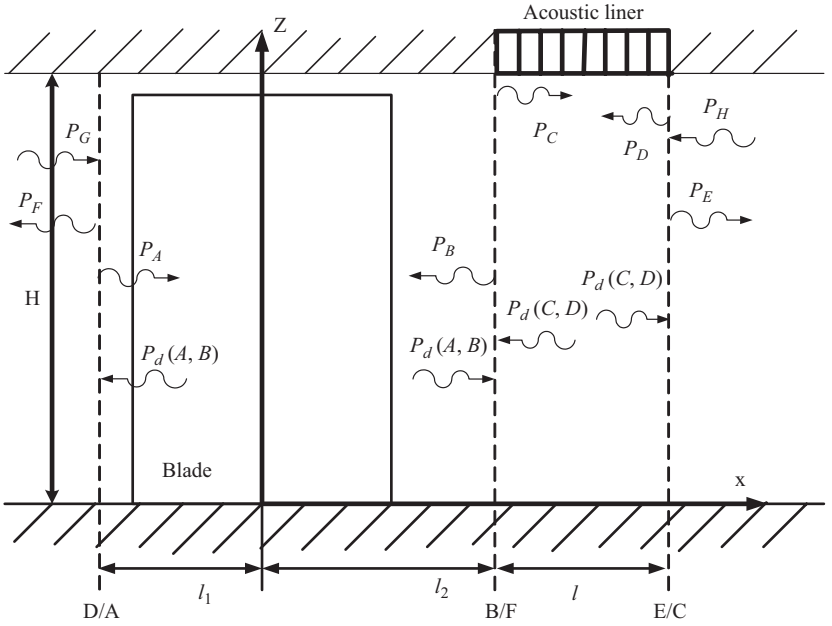

Fig. 14. Analysis model for OGV and the lined wall Section 3.

3. Numerical results and discussion

3.1. Comparison with the previous numerical results

In the present model in Fig. 2, when the value of wall impedance tends to be infinite, the model can be reduced to a blade row section model in Fig. 4. One of the theoretical results in the present analysis is the transmission and reflection coefficient. For comparison with Kaji and Okazaki [10], the three-dimensional equations can be reduced by letting radial wavenumber $k_n = 0$. And the result of solving three-dimensional integral equation for a hard wall will be the same as the two-dimensional model if the transmission and reflection coefficients are defined as

$$r_p = p_F/p_H, \tag{75}$$

$$t_p = p_E/p_H. \tag{76}$$

According to the above definition the correctness of the calculation method and program have been checked by comparison with the results of Kaji and Okazaki [10]. In the course of present study it is confirmed that the present method applied to the same conditions as used in Kaji and Okazaki's calculations gives results identical to theirs, as is seen in Fig. 6.

For checking the lined section, if the pressure differences between the lower and upper surface of blades are forced to be zero, the model can be reduced to a lined section model in Fig. 5. For comparison with Namba and Fukushige [5], the impedance model of the liner used in this paper is the same as the one used by Ko [21]. As is given by

$$Z = R(1 + \mathrm{i}\omega/\omega_0) - \mathrm{i}\cot(\omega d), \tag{77}$$

where R and ω_0 are the specific acoustic resistance and dimensionless characteristic angular frequency of the facing sheet, respectively, and d is the dimensionless depth of the honeycomb cavities.

One of the theoretical results in the present analysis is the sound power attenuation. In the course of present study it was confirmed that the present prediction gives a good agreement with Namba's calculations [5].

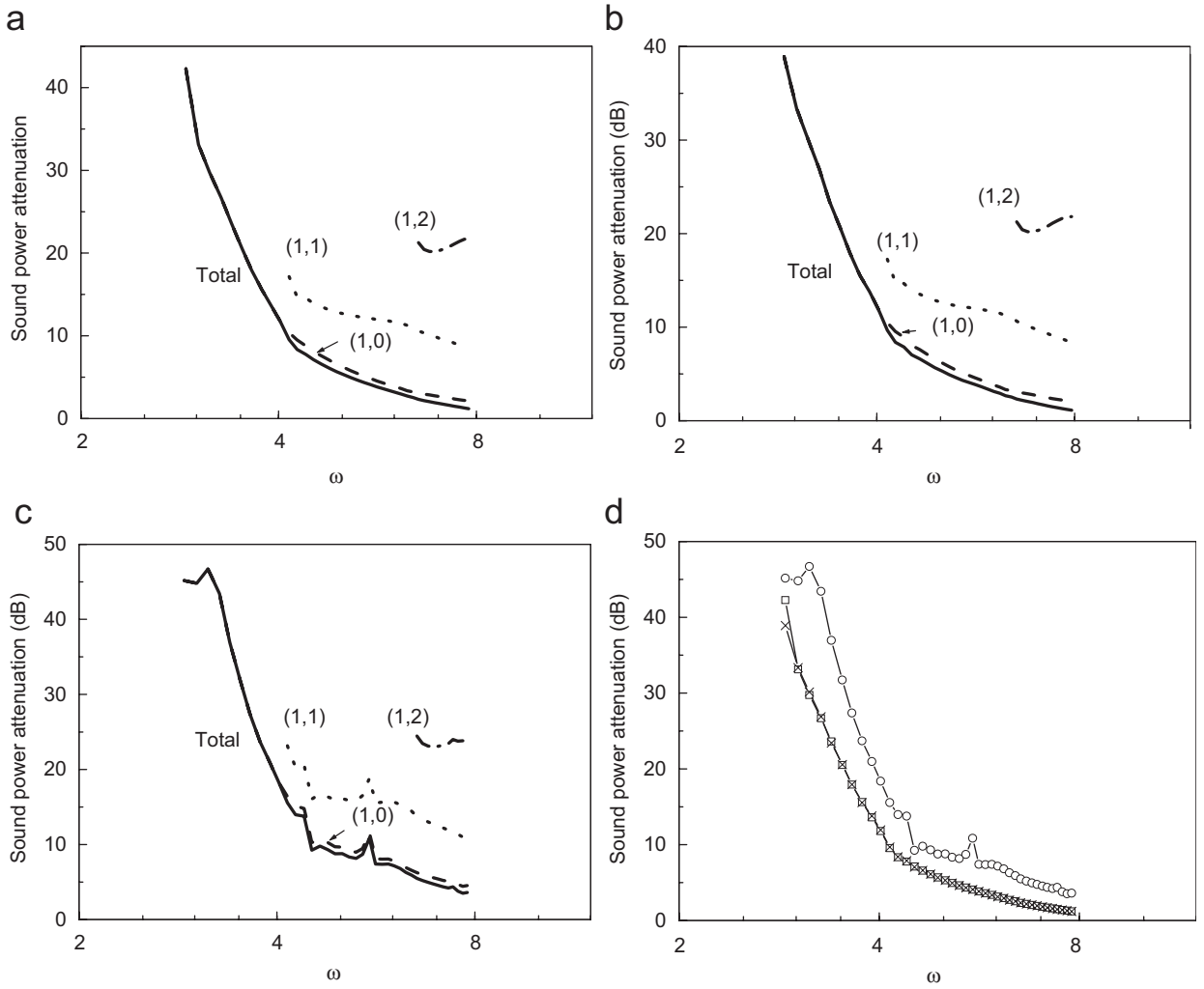

Fig. 15. (a) Modal spectra of the sound attenuation of the liner in Fig. 14 for the (1,0) mode incident from upstream side. (b) Effect of a cascade on the sound attenuation of the liner. (c) Modal spectra of the sound attenuation of the combination of the liner and the cascade. (d) The comparison of the total sound attenuation in (a)–(c), –□– total sound attenuation of case (a), – × – total sound attenuation of case (b), –○– total sound attenuation of case (c). $M_r = 0.4$, $l = 4.339$, $s/c = 1.0$, (1,0), (1,1) and (1,2) in (a)–(c) represent the cut-on modes corresponding to the given frequency.

A case is given in Fig. 7 when the incident wave is the fundamental (0,0) mode and there is no mean flow. For the same incident wave, Fig. 8 shows the comparison with Namba's results under different Mach number mean flow. As seen in Figs. 7 and 8, the agreement with each other is very good.

3.2. Numerical results for a combination of a blade row and liner sections

The effects of a blade row on sound propagation through a liner section and the real sound attenuation of the combination of the blade row and liner sections are investigated by using transfer element method for the three-dimensional flow filed. For all the examples calculated in this paper below, some parameters are set by the fixed value, such as $h/c = 0.5$, $R = 1.5$, $d = 0.271$, $\omega_0 = 25.86$, $\sigma = 0$, $\theta = 0^\circ$, and the dimensionless length $l_1 = l_2 = 1.0001$.

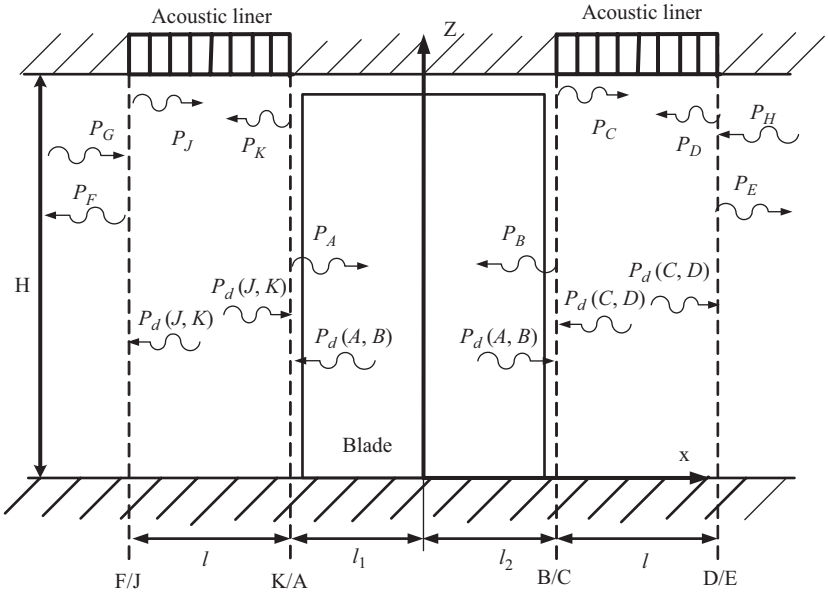

Fig. 16. Analysis model for OGV and the lined wall Sections 2 and 3.

3.2.1. Effect of a blade row on the sound attenuation of an upstream liner

The first example, shown in Fig. 2, is the sound propagation through a blade row and a liner section in the upstream side. Fig. 9 shows the numerical results of the sound power attenuation in the duct with the liner section only, the effect of the cascade on the sound attenuation of the liner, the real sound attenuation of the combination of the both sections, and the comparison of the total sound attenuation in the three cases for the (1,0) mode incident from upstream side. As is seen from Fig. 9(b) that the blade row has very little influence on the sound attenuation of the liner section. One point worth noting is that the effect of the blade row itself on the sound attenuation of the liner can be seen clearly when the reduced frequency is 2.89, on which the difference approaches 3.4 dB as shown in Fig. 9(d). But for most other frequencies, the differences are unidentifiable. However, the curve of the case with both the cascade and the liner deviates strikingly from that of the case with the liner only, as is seen from Fig. 9(d). For the range of reduced frequencies from 3.02 to 3.64, the differences of the sound attenuation between each other have exceeded 10 dB. And for most of the range, the differences are over 3 dB. This actually means that the insert of the cascade results in a positive effect on the sound attenuation for all the range of reduced frequencies.

Although the above example only presents a very little effect of the cascade on the sound attenuation of the liner, in some cases, for instance, when $s/c = 0.9$ or 1.1, the blade row has in fact a considerable effect on the performance of the liner. Fig. 10 ($s/c = 0.9$) has shown that the cascade, as a secondary source, strengthened the sound attenuation of the liner distinctively for the range of reduced frequency from 3.2 to 4.1. Especially for the reduced frequency of 3.2, the augment of sound attenuation has approached 23 dB. In contrast, for the case $s/c = 1.1$, Fig. 11 shows that the cascade weaken the sound attenuation of the liner obviously for the range of reduced frequency from 2.89 to 3.9. Especially for the reduced frequency of 2.89, the decrease of sound attenuation has approached 18 dB. But for most other high frequencies, the effect of the cascade becomes unidentifiable.

When the (1,1) mode sound wave impinges upon the cascade from downstream, the sound attenuation decreases distinctively compared to the (1,0) mode incidence. The blade row also has a very little effect on the sound attenuation of the liner section, which is shown in Fig. 12(b). As similar as the case in Fig. 9, in a certain range of reduced frequencies from 5.47 to 8.14 in Fig. 12(d), the insert of blade row strengthens the total sound attenuation in the duct obviously. And for the whole range of reduced frequencies, it shows a considerable increase on the sound attenuation in the duct.

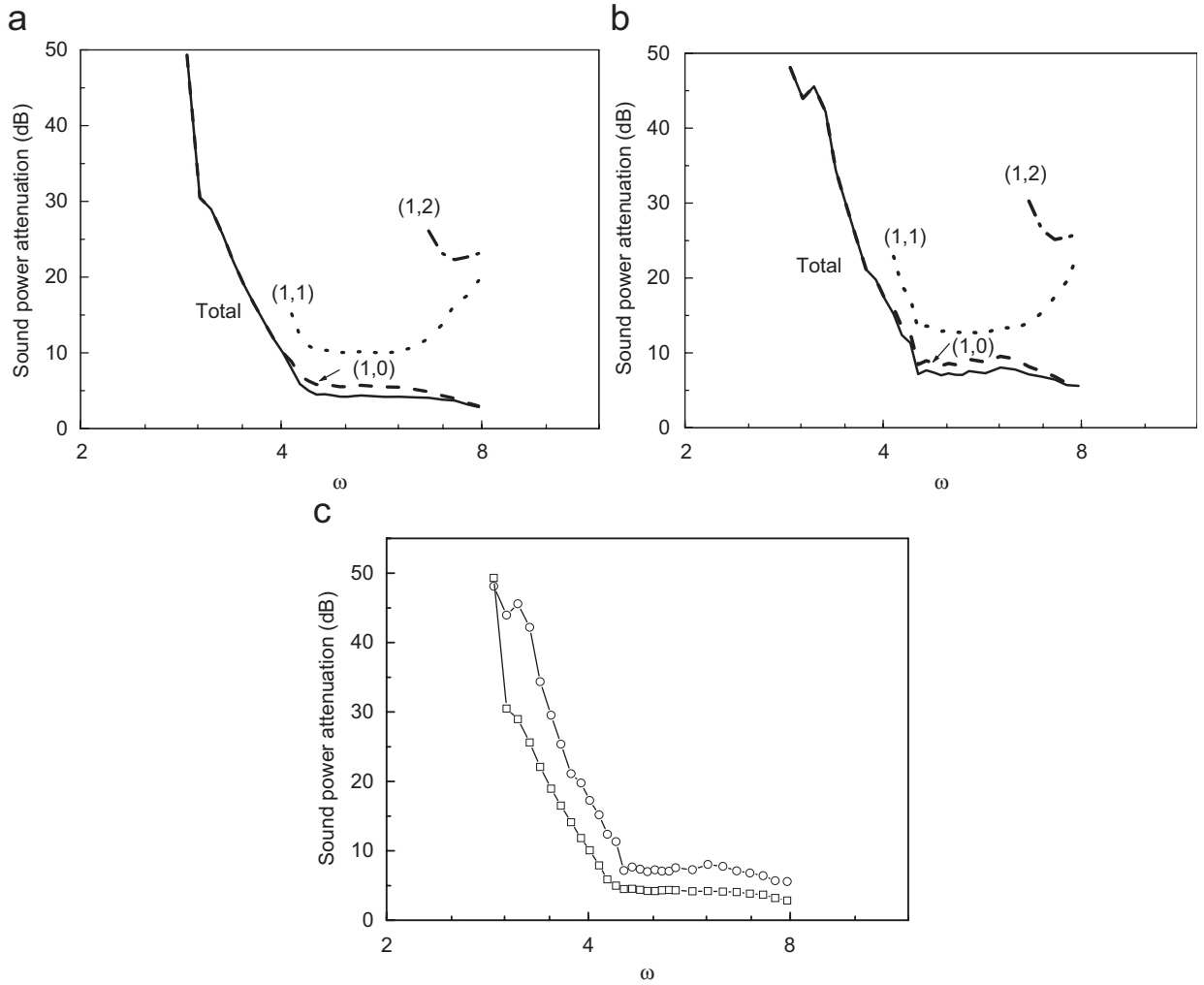

Fig. 17. (a) Modal spectra of the sound attenuation of the two lined wall section in Fig. 14 without cascade for the (1,0) mode incident from upstream side. (b) Modal spectra of the sound attenuation of the combination of the liners and the cascade. (c) The comparison of the total sound attenuation in (a) (b), –□– total sound attenuation of case (a), –○– total sound attenuation of case (b). $M_r = 0.4$, $l = 4.339$, $s/c = 1.0$, (1,0), (1,1) and (1,2) in (a)–(c) represent the cut-on modes corresponding to the given frequency.

Fig. 13 shows the numerical results for the mode (1,0) incident at high Mach number. With the increase of flow Mach number, the sound attenuation is weakened in the duct. And it presents an obvious fluctuation on the curves of the total sound attenuation seen in Fig. 13(d).

3.2.2. *Effect of a blade row on the sound attenuation of a downstream liner*

The second example (see Fig. 14) is the sound propagation through a cascade and a liner section in the downstream side. The numerical results in Fig. 15 for the (1,0) mode incident from upstream side show the similar trend as the case discussed above. For the whole range of reduced frequencies, the combination of the cascade and the liner section in the downstream side also brings out a considerable increase on the sound attenuation in the duct. And it should be noted that the difference between the sound attenuation of this sort of combination (the liner in the downstream side) and that of the combination mentioned above (see Fig. 2) is imperceptible. In other words, the effect of the position of liner (in the upstream side or downstream side) on the sound attenuation in the duct is not significant for the case discussed in this paper.

3.2.3. Effect of a blade row on the sound attenuation of two liner sections

The third example, shown in Fig. 16 is the combination of a blade row and two lined wall sections in the upstream and downstream side of the blade row, respectively. In order to compare with the results of previous examples, the length of the liner in this example is set by a half of that in the previous examples. For the (1,0) mode incident from upstream side, Figs. 17(a) and (b) show the sound attenuation of the two liner sections in the duct without cascade and that of the combination of cascade and liner sections, respectively. As shown in Fig. 17(c), the combination of the cascade and the two liner sections also has a positive effect on the sound attenuation for almost the whole range of cut-on frequencies.

In all the three examples when $s/c = 1.0$, the same conclusion that the insert of cascade always results in a positive effect on the sound attenuation in the duct with acoustic treatment could be achieved. The numerical results shown in these examples may be physically explained by the mechanism of vortex sound interaction [22,23], which tell us that the existence of a Kutta condition at the edge of a rigid surface in a flow causes the shedding of fluctuating vorticity if the flow is slightly unsteady, and the this process can extract energy from the sound field to form vortex which will be dissipated in flow fields. The Kutta condition is used in the present investigation, therefore, the energy dissipation caused by the vortex shedding at the edge of OGV enhances the sound attenuation in the duct with lined walls.

In order to further investigate the influence of OGV on the sound attenuation in the duct, the effect of space-chord ratio on sound propagation is studied in this paper. Numerical results in Fig. 18 show that by varying the space-chord ratio to a comparative low value one can obtain a considerable increase of sound attenuation without any change of liner section. In fact, the increase comes from two parts of contribution due to different mechanisms. On the one hand, with the variation of the space-chord ratio, the effect of OGV acting as the secondary source becomes more considerable on the sound attenuation of the liner. On the other hand, a certain benefit is derived from the vortex shedding of the OGV.

3.2.4. Effect of wake-blade row interactions on the liner sound attenuation

The last point worth considering is the power attenuation of sound propagation due to the wake from upstream. A convected sinusoidal wake perturbation including an upwash velocity of the reference blade gives

$$w(x,t) = -\bar{w}e^{i(\omega t - i\lambda\xi)}, \tag{78}$$

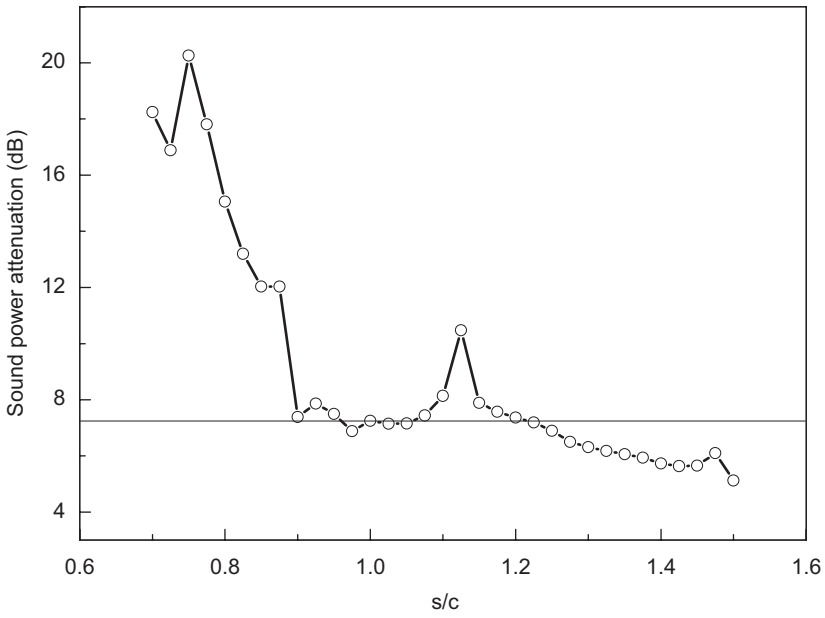

Fig. 18. Effect of the space-chord ratio s/c. –○– total sound attenuation of the combination of the two liner sections and the cascade for the (1,0) mode incident from upstream side, — the result for $s/c = 1$. $M_r = 0.4$, $l = 2.1695$.

where $\bar{w}$ represents the amplitude of upwash velocity, and the frequency parameter λ is given by

$$\lambda = 2\omega b/U_r. \tag{79}$$

In the present paper, the amplitude of upwash velocity is assumed to be equal to 1.0 at each Mach number. Figs. 19(a) and (b) show the sound attenuation of the liner section in the upstream side and downstream side, respectively, for the wake incident mentioned above. It has been shown that the peak points of power

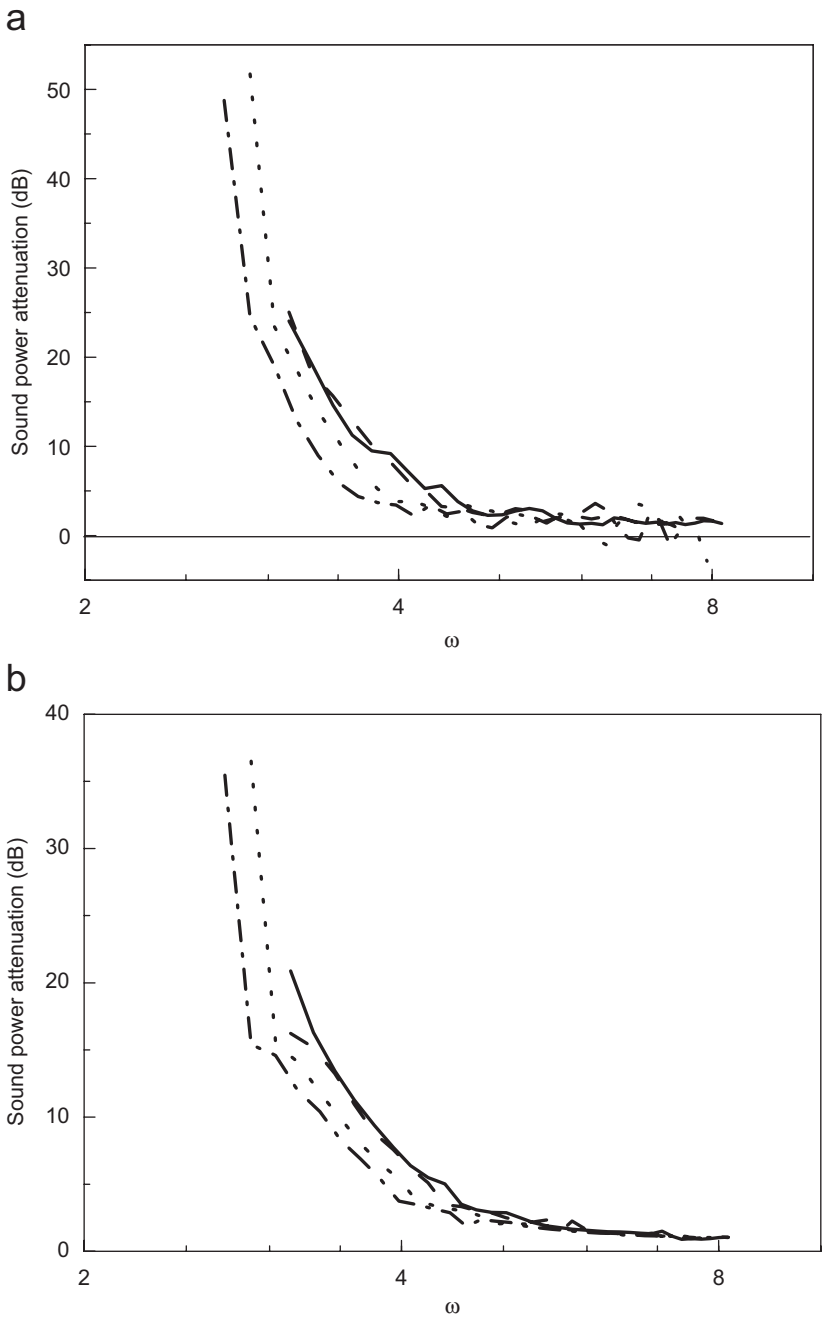

Fig. 19. Effect of flow Mach number for the wake incident: (a) sound power attenuation of the upstream liner; (b) sound power attenuation of the downstream liner. $l = 2.1695$, $s/c = 1$. — $M_r = 0.1$, – – $M_r = 0.2$, - - - $M_r = 0.4$, –·– $M_r = 0.5$.

attenuation at different Mach numbers appears on different frequencies due to the cut-off condition in the duct. For the liner section in the upstream side, when the Mach number is 0.4, the peak value of power attenuation has approached 51.72 dB on the reduced frequency of 2.88. However, it should be noted that the curves are very steep especially at high Mach number. When the reduced frequency is changed to 3.51 at a comparative high Mach number 0.4, only 10.375 dB can be achieved for this case. Even on some high frequencies, the liner has no effect on the sound attenuation at high Mach number with the given parameters in this example. The curves for the liner in the downstream side have the similar trend as that for the liner in the upstream side, but the value of the sound attenuation for the high Mach number is a little bit lower.

4. Conclusions

A model of sound propagation through a lining section and a blade row is developed to investigate the interaction between sound sources of blade rows and liners in a channel of parallel walls containing uniform mean flow. The present method makes it possible to evaluate the real sound attenuation in the duct with lined wall and cascades. Various numerical results show that the effect of the cascade may have diverse effects on sound attenuation of the liner under different conditions, but the existence of the OGV always enhances the total sound attenuation in the duct due to the energy dissipation caused by vortex shedding from the tailing edge of the OGV. To pursue a better design of acoustic liner in aeroengine nacelle, it is thus necessary to include the effect of OGV on the sound attenuation.

Acknowledgments

This work was supported by NSFC under Grant 50136010.

References

[1] E. Envia, *Fan noise reduction: an overview*, AIAA-2001-0661, 2001.
[2] D.L. Lansing, W.E. Zorumski, Effects of wall admittance changes on duct transmission and radiation of sound, *Journal of Sound and Vibration* 27 (1) (1973) 85–100.
[3] J.F. Unruh, Finite length tuning for low frequency lining design, *Journal of Sound and Vibration* 45 (1976) 5–14.
[4] W. Koch, Attenuation of sound multi-element acoustically lined rectangular ducts in the absence of mean flow, *Journal of Sound and Vibration* 52 (1977) 459–496.
[5] M. Namba, K. Fukushige, Application of the equivalent surface source method to the acoustics of duct systems with non-uniform wall impedance, *Journal of Sound and Vibration* 73 (1) (1980) 125–146.
[6] W. Eversman, Theoretical models for duct acoustics propagation and radiation, *Aeroacoustics of Flight Vehicles: Theory and Practice*, Vol. 2, NASA RP 1258, 1991, pp. 101–164 (Chapter 13).
[7] Y. Ozyoruk, L.N. Long, *T*ime-domain calculation of sound propagation in lined ducts with sheared flow, AIAA99-1817, 1999.
[8] Y. Ozyoruk, V. Ahujia, L.N. Long, Time domain simulation of radiation from ducted fans with liners, AIAA2001-2171, 2001.
[9] S. Kaji, T. Okazaki, Propagation of sound waves through a blade row I. Analysis based on the semi-actuator disk theory, *Journal of Sound and Vibration* 11 (3) (1970) 339–353.
[10] S. Kaji, T. Okazaki, Propagation of sound waves through a blade row II. Analysis based on the acceleration potential method, *Journal of Sound and Vibration* 11 (3) (1970) 355–375.
[11] R.S. Muir, The application of a semi-actuator disk model to sound transmission calculations in turbomachinery, part I: The single blade row, *Journal of Sound and Vibration* 54 (3) (1977) 393–408.
[12] R.S. Muir, The application of a semi-actuator disk model to sound transmission calculations in turbomachinery, part II: Multiple blade rows, *Journal of Sound and Vibration* 55 (3) (1977) 335–349.
[13] W. Koch, On the transmission of sound waves through a blade row, *Journal of Sound and Vibration* 18 (1) (1971) 111–128.
[14] R. Amiet, W.R. Sears, Reflection and transmission of oblique sound waves by a blade row, NASA SP-207, 1969, pp. 223–230.
[15] D.S. Whitehead, Vibration and sound generation in a cascade of flat plates in subsonic flow, ARC Reports and Memoranda No. 3685, 1970.
[16] F. Lane, M. Friedman, Theoretical investigation of subsonic oscillating blade-row aerodynamics, N.A.C.A. TN 4136, 1958.
[17] X. Sun, S. Kaji, Control of blade flutter using casing with acoustic treatment, *Journal of Fluids and Structure* 16 (5) (2002) 627–648.
[18] X. Sun, S. Kaji, Effects of wall admittance changes on aeroelastic stability of turbomachines, *AIAA Journal* 38 (9) (2000) 1525–1533.
[19] W.E. Zorumski, Acoustic theory of axisymmetric multisection ducts, NASA TM-R-419, May 1974.

[20] M.E. Goldstein, *Aeroacoustics*, McGraw-Hill, New York, 1976.
[21] S.-H. Ko, Sound attenuation in lined rectangular ducts with flow and its application to the reduction of aircraft engine noise, *Journal of the Acoustical Society of America* 50 (6) (1971) 1418–1432.
[22] M.S. Howe, *Acoustics of Fluid– Structure Interactions*, Cambridge University Press, Cambridge, 1998.
[23] D.W. Bechert, Sound absorption caused by vorticity shedding, demonstrated with a jet flow, *Journal of Sound and Vibration* 70 (3) (1980) 389–405.